East European Journal of Physics. 3. 292-297 (2026)
DOI:10.26565/2312-4334-2026-3-24 ISSN 2312-4334

BIDIRECTIONAL BAND GAP MODULATION IN ZnO-BASED THIN FILMS VIA CATION AND ANION-INDUCED LATTICE ENGINEERING

Javohir Sh. Khudoykulov[1]*, Shavkat U. Yuldashev[1,2], Azamat O. Arslanov[1], Jamoliddin X. Murodov[2], Andrey A. Nebesniy[1], Noiba U. Botirova[2], Ra'no Sh. Sharipova[2]
[1]*Department of Physics, National University of Uzbekistan, University Street 4, Tashkent 100174, Uzbekistan*
[2]*Center for Nanotechnologies Development, National University of Uzbekistan, University Street 4, Tashkent 100174, Uzbekistan*
**Corresponding Author email: xjavokhir1799@gmail.com*
Received April 13, 2026; revised June 22, 2026; accepted June 25, 2026

$Zn_{1-x}Mg_xO$ and $ZnO_{1-\gamma}S_\gamma$ thin films were synthesized by ultrasonic spray pyrolysis (USP) and investigated to achieve bidirectional band gap engineering in ZnO-based materials. X-ray diffraction confirmed a single-phase wurtzite structure with strong c-axis orientation for all samples. Mg incorporation induced a shift of the (002) peak toward higher angles, indicating lattice contraction, whereas S substitution caused a shift toward lower angles, corresponding to lattice expansion. UV–Vis analysis revealed a systematic blue shift of the band gap with Mg doping (from ~3.26 eV to ~3.33 eV) and a red shift with S incorporation (down to ~3.01 eV). These changes are attributed to lattice deformation and its influence on the electronic structure. Additionally, increased dopant concentration led to reduced crystallite size and increased microstrain and disorder. The results establish a clear correlation between lattice deformation and optical band gap modulation, demonstrating an effective approach for tuning ZnO-based thin films for optoelectronic applications.
Keywords: *ZnMgO; ZnOS; Band gap; Lattice deformation; Tauc plot; USP*

INTRODUCTION

ZnO is an II–VI semiconductor with a wide direct band gap of ~3.3 eV at room temperature and a large exciton binding energy (~60 meV), which makes it a promising material for optoelectronic applications such as ultraviolet (UV) lasers, light-emitting diodes, and photodetectors [1]. One of the most effective approaches to tailor its electronic and optical properties is alloying with suitable elements. In particular, Mg incorporation into ZnO leads to band gap widening due to the substitution of Zn^{2+} ions with smaller Mg^{2+} ions, resulting in lattice contraction and modification of the electronic band structure. This tunability is essential for the design of heterojunctions, quantum wells, and transparent optoelectronic devices [2].

In addition to cation substitution, anion substitution provides an alternative pathway for band-gap engineering. The incorporation of sulfur into ZnO ($ZnO_{1-\gamma}S_\gamma$) leads to lattice expansion due to the larger ionic radius of S^{2-} ions, typically resulting in band gap narrowing. Although ZnMgO and $ZnO_{1-\gamma}S_\gamma$ thin films have been widely studied using various deposition techniques, such as sol–gel processing, spray pyrolysis, pulsed laser deposition, and magnetron sputtering, a unified and quantitative understanding of the relationship among lattice deformation, microstructural disorder, and optical band gap modulation remains incomplete [3,4]. In particular, direct experimental comparison of cation- and anion-induced lattice effects within a single framework is still limited.

In this work, we systematically investigate the structural and optical properties of $Zn_{1-x}Mg_xO$ and $ZnO_{1-\gamma}S_\gamma$ thin films deposited on Si(100) substrates by ultrasonic spray pyrolysis (USP). X-ray diffraction (XRD) is employed to analyze crystal structure, lattice parameters, strain, and crystallite size, while UV–Vis spectroscopy is used to determine the optical band gap and Urbach energy [5]. By correlating lattice deformation with optical properties, this study aims to establish a comprehensive framework for bidirectional band gap engineering in ZnO-based thin films.

By combining qualitative figure analysis with the data, this study establishes a clear structure–property relationship, demonstrating how lattice contraction and expansion directly govern band gap widening and narrowing in ZnO-based alloys.

MATERIALS AND METHODS

ZnO-based thin films-undoped, Mg-doped (x = 0.05, 0.10), and S-doped (y = 0.05, 0.10) were deposited on Si(100) substrates by ultrasonic spray pyrolysis (USP). Aqueous precursor solutions were prepared from zinc acetate dihydrate, $Zn(C_2H_3O_2)_2{\cdot}2H_2O$ (0.5 mol/L). For Mg incorporation, magnesium acetate tetrahydrate, $(C_2H_3O_2)_2Mg{\cdot}4H_2O$, was added to achieve the desired Mg/(Zn+Mg) ratios; for S incorporation, thiourea, $SC(NH_2)_2$, was used as the sulfur source. Prior to deposition, Si(100) substrates were sequentially cleaned for 10 minutes each in hydrofluoric acid (10 % in DI) to remove the native SiO_2 layer, acetone and then ethanol to eliminate organic contaminants, followed by a final rinse in deionized (DI) water to remove residual species. All steps were performed under ultrasonic agitation to enhance cleaning efficiency [6-8]. Oxygen (O_2) at a flow of 500 sccm served as the carrier gas. The precursor aerosol was generated using a 1.7 MHz ultrasonic nebulizer and delivered to substrates maintained at 450 °C. After growth, all films were annealed at

Cite as: J.Sh. Khudoykulov, Sh.U. Yuldashev, A.O. Arslanov, J.X. Murodov, A.A. Nebesniy, N.U. Botirova, R.Sh. Sharipova, East Eur. J. Phys. 3, 292 (2026), https://doi.org/10.26565/2312-4334-2026-3-24

600°C for 15 minutes. The resulting thickness was approximately 200 nm. The experimental setup used in this work is illustrated in Figure 1. [10,11]

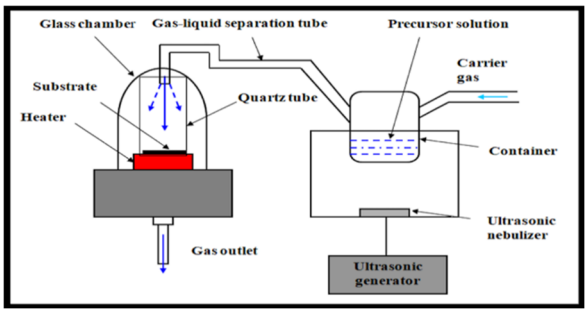

Figure 1. Scheme of Ultrasonic Spray Pyrolysis (USP)

Structural and optical characterization. X-ray diffraction (XRD) was carried out on a Rigaku MiniFlex diffractometer using Cu Kα radiation (λ = 1.5406 Å) over a 2θ range of 30°-60°. The average crystallite size was estimated from the full width at half maximum (FWHM) of the (002) reflection using the Scherrer relation. Optical absorption was measured with a UV-Vis spectrometer in the 300–500 nm wavelength range.[9] Surface morphology and grain structure were examined by field-emission scanning electron microscopy operated at 30 kV in secondary-electron mode using an Everhart–Thornley detector. Plan-view micrographs were spatially calibrated from the instrument pixel size (0.899 nm/px and 1.124 nm/px for the ZnMgO and ZnOS micrographs, respectively). Grain-size distributions were extracted by marker-controlled watershed segmentation, and the maximum Feret diameter was recorded for each grain (N ≥ 284 grains per sample); the distributions were described by a log-normal function.

RESULTS AND DISCUSSION

Figure 2 (a) shows the x-ray diffraction patterns of undoped ZnO and Mg doped $Zn_{1-x}Mg_xO$ thin films deposited on Si(100). All samples indicate a dominant diffraction peak corresponding to the (002) plane of hexagonal wurtzite ZnO, showing a strong preferential orientation along the c-axis. The absence of additional diffraction peaks related to MgO or other secondary phases confirms that Mg incorporation does not lead to phase segregation within the detection limit of XRD. With increasing Mg content, the (002) peak shifts slightly to higher 2θ values, indicating lattice contraction due to Mg substitution.[12]

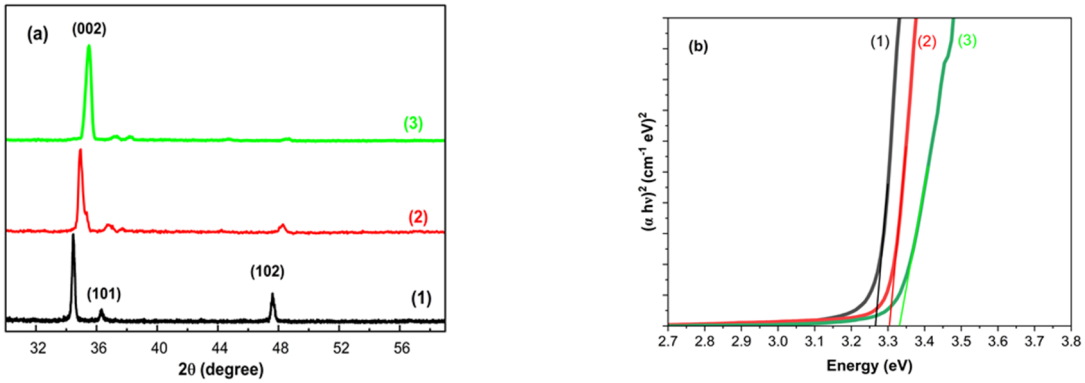

Figure 2. (a) XRD patterns and (b) Tauc plots of $Zn_{1-x}Mg_xO$ films grown on Si by USP; curves (1), (2), and (3) correspond to 0%, 5%, and 10% Mg, respectively

Figure 2 (b) shows the Tauc plots of $(\alpha h\nu)^2$ as a function of photon energy (hν) for undoped ZnO and Mg-doped $Zn_{1-x}Mg_xO$ thin films. The linear regions of the plots confirm that all films exhibit a direct allowed optical transition characteristic of the wurtzite ZnO crystal structure. As shown in Fig. 2(b), the absorption edge shifts progressively toward higher photon energies as the Mg concentration increases, indicating a systematic blue shift of the band gap. The extracted band gap values increase from 3.26 eV for undoped ZnO to 3.30 eV and 3.33 eV for 5% and 10% Mg-doped films, respectively, as summarized in Table 1. The observed band gap widening can be attributed to Mg-induced modification of the electronic band structure, which increases the energy separation between the conduction and valence bands [13].

Table 1. Some essential lattice parameters of ZnMgO thin film

Con. (%)	[002] (°)	FWHM (°)	c (Å)	E_g (eV)	D_{avg} (Å)	ε 10^{-3}	E_u (eV)
0	34.469	0.21541	5.199	3.26	340.55	3.03	0.180
5	34.949	0.34198	5.130	3.30	215.20	4.7	0.210
10	35.465	0.40687	5.058	3.33	150.821	5.5	0.235

The quantitative structural parameters extracted from Fig. 2(a) are summarized in Table 1 and provide strong support for the observed diffraction trends. As the Mg concentration increases from 0% to 10%, the (002) peak position shifts from 34.469° to 35.465°, confirming a continuous lattice contraction. Correspondingly, the calculated c-lattice parameter decreases significantly from 5.199 Å to 5.058 Å, which is consistent with Vegard's law behavior and reflects the smaller ionic radius of Mg^{2+} compared to Zn^{2+}. In addition to peak shifting, Fig. 2(a) shows noticeable peak broadening with increasing Mg content. This effect is quantified in Table 1 by the increase in full width at half maximum (FWHM) from 0.215° for pure ZnO to 0.407° for the 10% Mg-doped film.

The average crystallite size calculated from the (002) peak using the Debye–Scherrer equation:

$$D = 0.9\,\lambda / (\beta \cos\theta). \quad (1)$$

D_{avr} decreases dramatically from 340.55 Å to 150.82 Å as Mg concentration increases. This grain refinement is a direct consequence of Mg-induced strain and inhibited grain growth during film deposition. Despite this reduction in crystallite size, the films retain a strong c-axis orientation, indicating that Mg incorporation affects microstructural features without destroying overall crystallographic alignment.

The strain (ε) and dislocation density (δ) were calculated as:

$$\varepsilon = \beta / (4 \tan\theta),\ \delta = 1 / D^2. \quad (2)$$

The evolution of microstrain (ε) further supports this interpretation. As shown in Table 1, ε increases from 3.03×10^{-3} to 5.5×10^{-3} with Mg content, reflecting enhanced lattice distortion arising from ionic size mismatch and local compositional fluctuations. The simultaneous increase in Urbach energy (E_u) from 0.178 eV to 0.235 eV suggests an increase in localized states and structural disorder, which correlates well with the observed peak broadening and strain evolution. These calculations confirm that ZnMgO films possess nanocrystalline grains with low dislocation density, suitable for optoelectronic integration.

Figure 3 presents the structural and optical evolution of $ZnO_{1-x}S_x$ thin films as a function of sulfur concentration. Figure 3(a) shows the XRD patterns, while Fig. 3(b) displays the corresponding Tauc plots used to extract the optical band gap. As seen in Fig. 3(a), increasing sulfur concentration results in a progressive shift of the (002) diffraction peak toward lower diffraction angles. This behavior indicates an increase in the interplanar spacing along the c-axis, suggesting lattice expansion induced by sulfur incorporation. The absence of secondary phases in the diffraction patterns confirms that sulfur is incorporated into the ZnO lattice without forming separate sulfide phases. The qualitative trends observed in Fig. 3(a) are quantitatively supported by the data summarized in Table 2. The c-axis lattice parameter increases systematically from 5.1999 Å for undoped ZnO to 5.2928 Å for 10% S, confirming a clear expansion of the wurtzite lattice. This lattice dilation originates from the substitution of O^{2-} ions by larger S^{2-} ions, which introduces tensile strain along the growth direction.

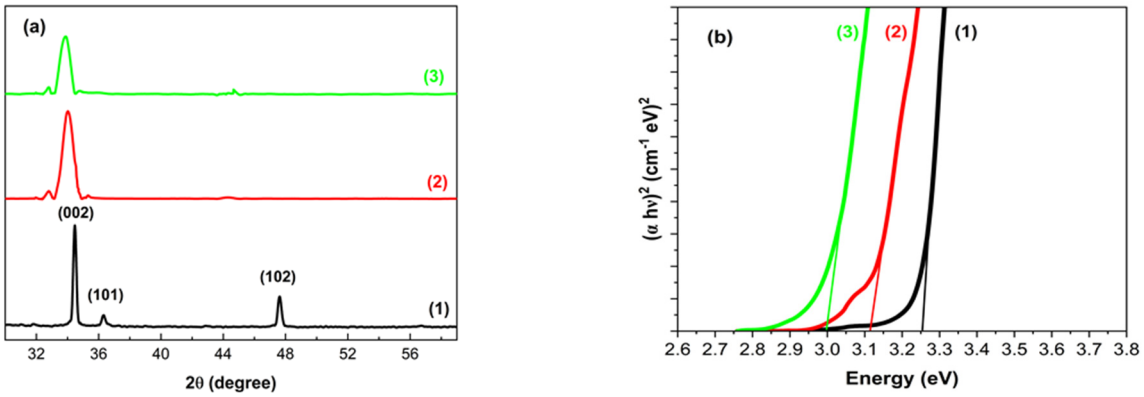

Figure 3. (a) XRD patterns and (b) Tauc plots of $ZnO_{1-x}S_x$ films grown on Si by USP; curves (1), (2), and (3) correspond to 0%, 5%, and 10%, respectively

Accordingly, Fig. 3(b) shows a continuous red shift in the optical absorption edge as the sulfur concentration increases. The extracted band gap values decrease from 3.26 eV (0%) to 3.01 eV (10%), as listed in Table 2.

Table 2. Some essential lattice parameters of ZnOS thin film

Con. (%)	[002] (°)	FWHM	c (Å)	E_g (eV)	D_{avg} (Å)	ε 10^{-3}	E_u (eV)
0	34.4696	0.21541	5.1999	3.26	340.55	3.03	0.180
5	34.0322	0.68788	5.2644	3.11	120.77	9.81	0.264
10	33.8442	0.77724	5.2928	3.01	106.87	11.1	0.292

This band gap narrowing is directly correlated with lattice expansion, as increased bond lengths reduce orbital overlap and modify the electronic band structure, thereby shifting the conduction band minimum downward. The inverse relationship between c-lattice parameter and optical band gap energy demonstrates that band gap modulation in $ZnO_{1-x}S_x$

films is strongly governed by structural deformation rather than compositional effects alone. As a result structural disorder leads to the significant increase in FWHM values, from 0.215° to 0.777°.

Table 2 reveals some microstructural parameters of material. The average crystallite size decreases sharply from 340.55 Å to 106.87 Å**,** while the microstrain increases from 3.03×10^{-3} to 11.1×10^{-3} with sulfur content. These changes reflect increasing internal stress and defect density within the lattice. Additionally, the Urbach energy (E_u) increases from 0.180 eV to 0.292 eV, indicating a higher density of localized states and enhanced band tailing caused by structural disorder. Overall, the combined analysis of Fig. 3 and Table 2 confirms that sulfur incorporation induces lattice expansion, increased strain, crystallite size reduction, and band gap narrowing in $ZnO_{1-x}S_x$ thin films. These results clearly demonstrate that controlled anion substitution provides an effective approach for tailoring the optical properties of ZnO-based materials, which is of significant interest for visible and UV optoelectronic applications.[13]

Figure 4 illustrates the correlation between the c-axis lattice parameter and the optical band gap energy for $Zn_{1-x}Mg_xO$ and $ZnO_{1-\gamma}S_\gamma$ thin films. A clear and systematic relationship is observed, demonstrating that lattice deformation plays a dominant role in governing the electronic structure of ZnO-based alloys.

For $Zn_{1-x}Mg_xO$ films, the c-axis lattice parameter decreases with increasing Mg concentration, indicating lattice contraction due to the substitution of Zn^{2+} ions by smaller Mg^{2+} ions. This structural compression leads to a widening of the band gap, which increases from ~3.26 eV to ~3.33 eV. The band gap expansion can be attributed to enhanced orbital overlap and increased energy separation between the conduction and valence bands caused by reduced interatomic spacing.

In contrast, $ZnO_{1-\gamma}S_\gamma$ films exhibit an opposite trend. The c-axis lattice parameter increases with increasing sulfur content, reflecting lattice expansion due to the larger ionic radius of S^{2-} ions compared to O^{2-} ions. This expansion results in a reduction of orbital overlap and a corresponding narrowing of the band gap, decreasing to ~3.01 eV. The observed red shift is associated with the modification of the valence band structure and increased localization of electronic states.

The nearly linear dependence between lattice parameter and band gap in both systems suggests Vegard's law-like behavior, confirming that compositional variation directly influences the structural and optical properties. Importantly, the opposite trends observed for Mg and S substitution highlight a bidirectional mechanism of band gap engineering, where lattice contraction and expansion provide two complementary pathways for tuning the optical response of ZnO-based thin films.

These results clearly demonstrate that precise control of lattice deformation through cation and anion substitution offers a powerful strategy for designing materials with tailored band structures for advanced optoelectronic applications.

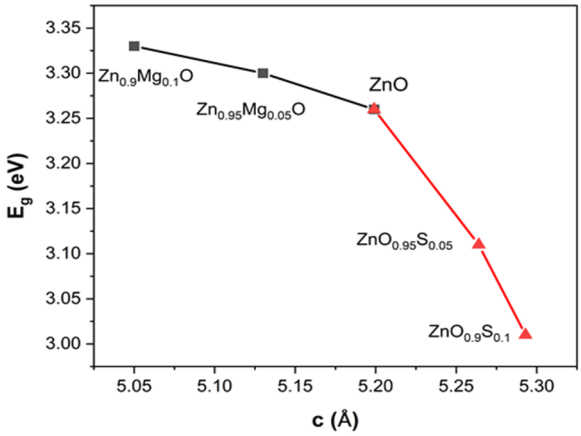

Figure 4. Band gap versus of $Zn_{1-x}Mg_xO$ and $ZnO_{1-\gamma}S_\gamma$ thin films c-axis lattice parameter

For comparison, $ZnO_{1-y}S_y$ alloys show the opposite trend: band gap narrowing and expansion of the c-lattice parameter, owing to the larger ionic radius of sulfur. These contrasting behaviors highlight the versatility of ZnO-based alloys for band-structure engineering.

Figure 5(a,c) presents plan-view SEM micrographs of the 10% Mg and 10% S films. Both surfaces are dense, continuous, and crack-free, displaying rounded, faceted grains with well-defined intergranular boundaries, consistent with the single-phase wurtzite structure revealed by XRD. No secondary-phase precipitates or pinholes are observed, confirming that Mg and S are incorporated without phase segregation at the film surface.[14]

The corresponding grain-size distributions [Fig. 5(b,d)] follow a log-normal profile, which is characteristic of nucleation-and-growth thin films. The $Zn_{0.9}Mg_{0.1}O$ film exhibits a median Feret diameter of 62.9 nm (mean 78.0 nm), whereas the $ZnO_{0.9}S_{0.1}$ film shows a larger median of 96.6 nm (mean 110.4 nm), as summarized in Table 3.

Importantly, the SEM grain sizes (≈60–100 nm) substantially exceed the X-ray crystallite sizes obtained from the Scherrer analysis (15.1 nm for 10% Mg and 10.7 nm for 10% S; Tables 1 and 2). This indicates that each SEM grain is a mesoscale aggregate composed of several coherently diffracting crystallites separated by low-angle sub-grain boundaries—that is, the two techniques probe different length scales. Notably, although the $ZnO_{0.9}S_{0.1}$ film has the larger mesoscale grains, it possesses the smaller crystallites together with the highest microstrain (11.1×10^{-3}) and Urbach energy

(0.292 eV). This apparent contrast is self-consistent: the larger sulfur-induced lattice expansion and tensile strain fragment each grain into smaller coherent domains and increase the density of localized states, while grain coalescence during growth still produces larger mesoscale grains. The morphology, therefore, corroborates the microstructural disorder inferred from the XRD and UV–Vis data [15].

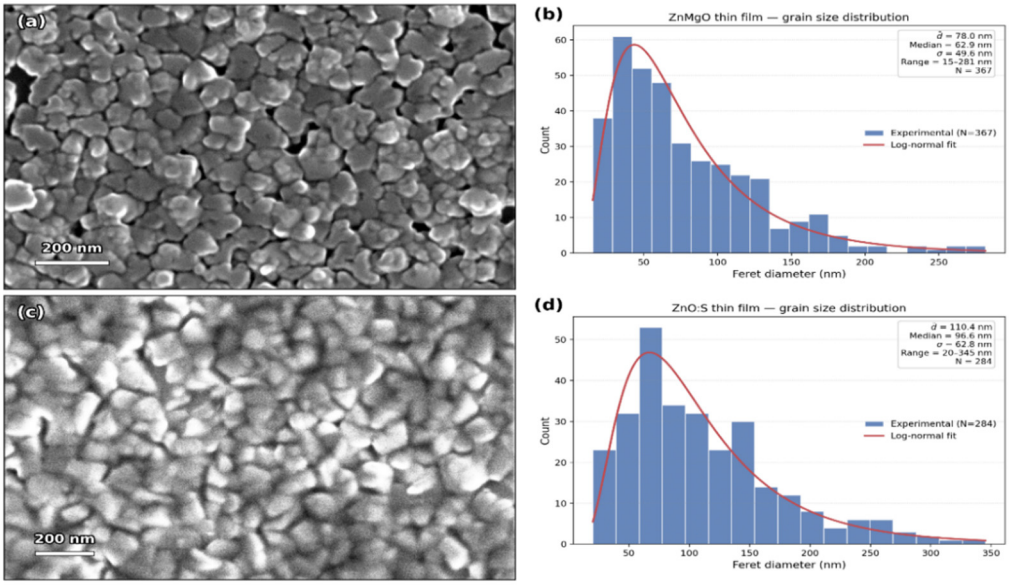

Figure 5. Plan-view SEM micrographs and corresponding grain-size distributions of (a, b) $Zn_{0.9}Mg_{0.1}O$ and (c, d) $ZnO_{0.9}S_{0.1}$ thin films grown on Si(100) by USP. Histograms show the maximum Feret diameter with a log-normal fit (red line); insets list the mean, median, standard deviation σ, range and grain count N. Scale bars: 200 nm

Finally, it should be emphasized that the optical band-gap modulation (Fig. 4) follows the composition-driven lattice deformation and crystallite-level disorder rather than the SEM grain size. At 60–100 nm the grains are far larger than the ZnO exciton Bohr radius (≈2.3 nm), so quantum size effects are negligible and the band gap is governed by the cation/anion substitution and the associated strain. The SEM analysis thus provides complementary morphological evidence that supports, but does not drive, the observed band-gap trends.

Table 3. Grain-size parameters (SEM, max Feret diameter) and crystallite size (XRD, Scherrer) of the 10% films.

Sample	Median Feret (nm)	Mean Feret (nm)	σ (nm)	N	XRD D (nm)	Grain/crystallite
$Zn_{0.9}Mg_{0.1}O$	62.9	78.0	49.6	367	15.1	~4.2
$ZnO_{0.9}S_{0.1}$	96.6	110.4	62.8	284	10.7	~9.0

D – average crystallite size from the (002) reflection (Tables 1–2). The grain/crystallite ratio illustrates that each SEM grain contains several coherent domains.

CONCLUSIONS

In this study, $Zn_{1-x}Mg_xO$ and $ZnO_{1-\gamma}S_\gamma$ thin films were successfully deposited on Si(100) substrates by ultrasonic spray pyrolysis, and their structural and optical properties were systematically investigated to clarify the role of cation and anion substitution in band gap engineering of ZnO-based alloys. X-ray diffraction analysis confirmed that all films exhibit a single-phase hexagonal wurtzite structure with strong preferential orientation along the c-axis, indicating successful incorporation of both Mg and S without the formation of secondary phases. Structural analysis revealed contrasting lattice responses: Mg incorporation resulted in lattice contraction, whereas S substitution produced lattice expansion, both consistent with the ionic radii of the respective substituents. These structural changes resulted in a bidirectional modulation of the optical band gap, with a systematic widening from ~3.26 eV to ~3.33 eV for $Zn_{1-x}Mg_xO$ and a narrowing down to ~3.01 eV for $ZnO_{1-\gamma}S_\gamma$. The correlation among lattice parameters, microstrain, crystallite size, and Urbach energy indicates that band-gap evolution is strongly governed by lattice deformation and associated structural disorder.

Plan-view SEM analysis confirmed that all films are dense, crack-free, single-phase polycrystalline layers with log-normal grain-size distributions, the median Feret diameter increasing from 62.9 nm for $Zn_{0.9}Mg_{0.1}O$ to 96.6 nm for $ZnO_{0.9}S_{0.1}$. These mesoscale grains are several times larger than the XRD crystallites, indicating that each grain comprises multiple coherent domains; the larger-grain yet smaller-crystallite, higher-strain character of the sulfur-doped film is fully consistent with the structural picture obtained from XRD and UV–Vis. The morphological results therefore reinforce that the bidirectional band-gap modulation is governed by composition-driven lattice deformation and microstructural disorder rather than by grain-size (quantum-confinement) effects.

The results establish a unified experimental framework linking lattice deformation to optical band gap tuning in ZnO-based thin films. This study highlights that controlled cation and anion substitution provides a versatile and effective route for tailoring the optoelectronic properties of ZnO alloys. Such tunability makes these materials highly promising for applications in ultraviolet and visible photodetectors, transparent electronics, and band-engineered heterostructures.

ORCID

Javohir Sh. Khudoykulov, https://orcid.org/0009-0005-4223-8863**; Shavkat U. Yuldashev,** https://orcid.org/0000-0002-2187-5960; **Azamat O. Arslanov**, https://orcid.org/0009-0000-4817-8770; **Jamoliddin X. Murodov,** https://orcid.org/0009-0006-3088-4881; **Noiba U. Botirova,** https://orcid.org/0009-0002-2294-9981

REFERENCE

[1] Ü. Özgür, Y. I. Alivov, C. Liu, et al., "A comprehensive review of ZnO materials and devices," Journal of Applied Physics**, 98**, (2005) 041301. https://doi.org/10.1063/1.1992666

[2] A. Ohtomo, and M. Kawasaki, "ZnO-based heterostructures: MgZnO/ZnO quantum wells," Applied Physics Letters**, 72**, 2466-2468 (1998). https://doi.org/10.1063/1.121384

[3] S. Major, A. Banerjee, and K. L. Chopra, "Highly transparent and conducting ZnO films prepared by spray pyrolysis," Thin Solid Films**, 108**, 333–340 (1983). https://doi.org/10.1016/0040-6090(83)90438-5

[4] S. Pearton, D. Norton, K. Ip, et al., "Recent progress in processing and properties of ZnO," Progress in Materials Science**, 50**, 293–340 (2005). https://doi.org/10.1016/j.pmatsci.2004.04.001

[5] R. Vinodkumar, and K. Vijayalakshmi, "Effect of Mg incorporation on structural and optical properties of ZnMgO thin films," Materials Science in Semiconductor Processing**, 16**, 1–6 (2013). https://doi.org/10.1016/j.mssp.2012.08.004

[6] J. X. Murodov, Sh. U. Yuldashev, A. O. Arslanov, N. U. Botirova, J. Sh. Xudoyqulov, R. Sh. Sharipova, R. A. Nusretov, *et al*., "Resistive Switching Behavior of SnO_2/ZnO Heterojunction Thin Films for Non-Volatile Memory Applications," East Eur. J. Phys. (3), 348–352 (2025). https://doi.org/10.26565/2312-4334-2025-3-34

[7] R. Zhang, Sh. U. Yuldashev, J. C. Lee, V. Sh. Yalishev, T. W. Kang, and D. J. Fu, "Electrical Properties of ZnO Nanostructures Grown on Si Substrates," Microelectron. Eng. **112**, 31–35 (2013). https://doi.org/10.1016/j.mee.2013.05.018

[8] N. U.Botirova, A. O. Arslanov, G. B. Eshobqulov, J. X. Murodov, R. Sh. Sharipova, J. Sh. Xudoyqulov, and Sh. U. Yuldashev, "Effect of SiO_2 and Post-Annealed Ga_2O_3 Buffer Layers on Ga_2O_3 Thin Film Growth and Properties," Cryst. Growth Des. **25**(18), 7828–7833 (2025). https://doi.org/10.1021/acs.cgd.5c01075

[9] M. Caglar, S. Ilican, and Y. Caglar, "Influence of sulfur doping on structural and optical properties of ZnO thin films," Journal of Alloys and Compounds, **509**, 5130–5137 (2011). https://doi.org/10.1016/j.jallcom.2011.01.061

[10] A. Arslanov, Sh. Yuldashev, N. Botirova, R. Nusretov, J. Murodov, and J. Xudoyqulov, "Impact of Precursor Molar Concentration on the Structural and Optical Properties of ZnO Thin Films Synthesized by Ultrasonic Spray Pyrolysis," Physical Science International Journal, **29**(1), 29-35 (2025). https://doi.org/10.9734/psij/2025/v29i1871

[11] Sh Yuldashev, K. Mukimov, G. Eshonkulov, A. Arslanov, and J. Xudoykulov, "Diluted Magnetic Semiconductors for Spintronics Applications," in: *ICLODAM-24*, (Tashkent, Uzbekistan, 2024).

[12] V. Morari, V.V. Ursaki, E.V. Rusu, V.V. Zalamai, P. Colpo, and I.M. Tiginyanu, "Spin-Coating and Aerosol Spray Pyrolysis Processed $Zn_{1-x}Mg_xO$ Films for UV Detector Applications," Nanomaterials, **12**, 3209 (2022). https://doi.org/10.3390/nano12183209

[13] H. Morkoç, AND Ü. Özgür, *Zinc Oxide: Fundamentals, Materials and Device Technology*, (Wiley-VCH, Weinheim, 2009).

[14] A. Janotti, AND C.G. Van de Walle, "Fundamentals of zinc oxide as a semiconductor," Reports on Progress in Physics**, 72**, 126501 (2009). https://doi.org/10.1088/0034-4885/72/12/126501

[15] *Transparent Conductive Zinc Oxide*, edited by K. Ellmer, A. Klein, and B. Rech, "Springer Series in Materials Science, 2008". https://doi.org/10.1007/978-3-540-73612-7

ДВОНАПРАВЛЕНА МОДУЛЯЦІЯ ШИРИНИ ЗАБОРОНЕНОЇ ЗОНИ В ТОНКИХ ПЛІВКАХ НА ОСНОВІ ZnO ЗА ДОПОМОГОЮ КАТИОННО-ТА АНІОННО-ІНДУКОВАНОЇ ГРАТКОВОЇ ІНЖЕНЕРІЇ

Джавохір Ш. Худойкулов[1], Шавкат У. Юлдашев[1,2], Азамат О. Арсланов[1], Джамоліддін Х. Муродов[2], Андрій А. Небесний[1], Нойба У. Ботірова[2], Ра'но Ш. Шаріпова[2]

[1]Кафедра фізики, Національний університет Узбекистану, вулиця Університетська, 4, Ташкент 100174, Узбекистан
[2]Центр розвитку нанотехнологій, Національний університет Узбекистану, вулиця Університетська, 4, Ташкент 100174, Узбекистан

Тонкі плівки $Zn_{1-x}Mg_xO$ та $ZnO_{1-\gamma}S_\gamma$ були синтезовані методом ультразвукового розпилювального піролізу та досліджені з метою досягнення двонаправленої інженерії забороненої зони в матеріалах на основі ZnO. Рентгенівська дифракція підтвердила однофазну структуру вюрциту з сильною орієнтацією осі c у всіх зразках. Включення Mg викликало зміщення піку (002) до більших кутів, що вказує на стиснення решітки, тоді як заміщення S викликало зміщення до менших кутів, що відповідає розширенню решітки. UV–Vis аналіз виявив систематичний зсув ширини забороненої зони в синю область спектра при легуванні магнієм (від ~3,26 еВ до ~3,33 еВ) та зсув у червону область спектра при включенні сірки (до ~3,01 еВ).. Ці зміни пояснюються деформацією решітки та її впливом на електронну структуру. Крім того, збільшення концентрації легуючої домішки призвело до зменшення розміру кристалітів та збільшення мікродеформації та переупорядкування. Результати встановлюють чітку кореляцію між деформацією решітки та модуляцією оптичної забороненої зони, демонструючи ефективний підхід до налаштування тонких плівок на основі ZnO для оптоелектронних застосувань.

Ключові слова: *ZnMgO; ZnOS; ширина забороненої зони; деформація решітки; діаграма Таука; ультразвуковий піроліз*